
Transductive Information Maximization For Few-Shot Learning

Malik Boudiaf*
ÉTS Montreal

Ziko Imtiaz Masud
ÉTS Montreal

Jérôme Rony
ÉTS Montreal

José Dolz
ÉTS Montreal

Pablo Piantanida
CentraleSupélec
CNRS-Université Paris-Saclay

Ismail Ben Ayed
ÉTS Montreal

Abstract

We introduce Transductive Information Maximization (TIM) for few-shot learning. Our method maximizes the mutual information between the query features and predictions of a few-shot task, subject to supervision constraints from the support set. Furthermore, we propose a new alternating direction solver for our mutual-information loss, which substantially speeds up transductive-inference convergence over gradient-based optimization, while demonstrating similar accuracy performance. Following standard few-shot settings, our comprehensive experiments² demonstrate that TIM outperforms state-of-the-art methods significantly across all datasets and networks, while using simple cross-entropy training on the base classes, without resorting to complex meta-learning schemes. It consistently brings between 2% to 5% improvement in accuracy over the best performing methods not only on all the well-established few-shot benchmarks, but also on more challenging scenarios, with domain shifts and larger number of classes.

1 Introduction

Deep learning models have achieved unprecedented success, approaching human-level performances when trained on large-scale labeled data. However, the generalization of such models might be seriously challenged when dealing with new (unseen) classes, with only a few labeled instances per class. Humans, however, can learn new tasks rapidly from a handful of instances, by leveraging context and *prior* knowledge. The few-shot learning (FSL) paradigm [20, 6, 36] attempts to bridge this gap, and has recently attracted substantial research interest, with a large body of very recent works, e.g., [11, 5, 28, 40, 19, 3, 25, 14, 31, 39, 8, 29, 7], among many others. In the few-shot setting, a model is first trained on labeled data with *base* classes. Then, model generalization is evaluated in few-shot *tasks*, over unlabeled examples of novel classes unseen during training (the *query* set), assuming only one or a few labeled examples (the *support* set) are given per novel class.

Most of the existing approaches within the FSL framework are based on the “learning to learn” paradigm or meta-learning [7, 29, 36, 31, 16], where the training set is viewed as a series of balanced tasks (or *episodes*), so as to simulate test-time scenarios. Popular works include prototypical networks [29], which describes each class with an embedding prototype and maximizes the log-probability of query samples via episodic training; matching network [36], which represents query predictions as linear combinations of support labels and employs episodic training along with memory architectures; MAML [7], a meta-learner, which trains a model to make it “easy” to fine-tune; and the LSTM

*Corresponding author: malik.boudiaf.1@etsmtl.net

²Code publicly available at <https://github.com/mboudiaf/TIM>

meta-learner in [26], which suggests optimization as a model for few-shot learning. A large body of meta-learning works followed-up lately, to only cite a few [28, 24, 21, 31, 40].

1.1 Related work

In a very recent line of work, *transductive* inference has emerged as an appealing approach to tackling few-shot tasks [5, 11, 14, 19, 25, 23, 18, 42], showing performance improvements over *inductive* inference. In the transductive setting³, the model classifies the unlabeled query examples of a given few-shot task at once, instead of one sample at a time as in inductive methods. These recent experimental observations in few-shot learning are consistent with established facts in classical transductive inference [35, 13, 4], which is well-known to outperform inductive methods on small training sets. While [23] used information of unlabeled query samples via batch normalization, the authors of [19] were the first to model explicitly transductive inference in few-shot learning. Inspired by popular label propagation concepts [4], they built a meta-learning framework that learns to propagate labels from labeled to unlabeled instances via a graph. The meta-learning transductive method in [11] used attention mechanisms to propagate labels to unlabeled query samples. More closely related to our work, the very recent transductive inference of Dhillon et al [5] minimizes the entropy of network predictions at unlabeled query samples, reporting competitive few-shot performances, while using standard cross-entropy training on base classes. Its competitive performances are in line with several recent inductive baselines [3, 37, 33] reporting that standard cross-entropy training for the base classes matches or exceeds the performances of more sophisticated meta-learning procedures. The performance of [5] is in line with established results in the context of semi-supervised learning, where entropy minimization is widely used [9, 22, 1]. It is worth noting that the inference runtimes of transductive methods are, typically, much higher than their inductive counterparts. For, instance, the authors of [5] fine-tune all the parameters of a deep network during inference, which is several orders of magnitude slower than inductive methods such as ProtoNet [29]. Also, based on matrix inversion, the transductive inference in [19] has a complexity that is cubic in the number of query samples.

1.2 Contributions

We propose Transductive Information Maximization (TIM) for few-shot learning. Our method aims at maximizing the mutual information between the query features and predictions of a few-shot task at inference. In addition to standard gradient-based optimization, we derive a new Alternating Direction optimizer for our objective, which yields substantial speedup in transductive inference while maintaining similar level of accuracy. Following standard experimental few-shot settings, our comprehensive evaluations show that TIM outperforms state-of-the-art methods substantially across all datasets and networks, while used on top of a fixed feature extractor pre-trained with simple cross-entropy on the base classes. It consistently brings over 2% of improvement in accuracy over the best performing method in the 1-shot scenario, and between 3% to 5% improvement in the 5-shot scenario, not only on all the well-established few-shot benchmarks, but also on more challenging, recently introduced scenarios, with domain shifts and larger number of ways.

2 Transductive Information Maximization

2.1 Few-shot setting

Given a labeled training set: $\mathcal{X}_{\text{base}} := \{\mathbf{x}_i, \mathbf{y}_i\}_{i=1}^{N_{\text{base}}}$ where \mathbf{x}_i denotes raw features of sample i and \mathbf{y}_i its associated one-hot encoded label. Such labeled set is often referred to as the *meta-training* or *base* dataset in the few-shot literature. Let $\mathcal{Y}_{\text{base}}$ denote the set of classes for this base dataset. The few-shot scenario assumes that we are given a *test* dataset: $\mathcal{X}_{\text{test}} := \{\mathbf{x}_i, \mathbf{y}_i\}_{i=1}^{N_{\text{test}}}$, with a completely new set of classes $\mathcal{Y}_{\text{test}}$ such that $\mathcal{Y}_{\text{base}} \cap \mathcal{Y}_{\text{test}} = \emptyset$, from which we create randomly sampled few-shot *tasks*, each with a few labeled examples. Specifically, each K -way N_S -shot task involves sampling N_S labeled examples from each of K different classes, also chosen at random. Let \mathcal{S} denote the set of these

³Transductive few-shot inference is not to be confused with semi-supervised few-shot learning [27]. The latter uses extra unlabeled data during meta-training. Transductive inference has access to exactly the same training/testing data as its inductive counterpart, while leveraging the information shared by unlabeled samples.

labeled examples, referred to as the *support* set with size $|\mathcal{S}| = N_S \cdot K$. Furthermore, each task has a *query* set denoted by \mathcal{Q} composed of $|\mathcal{Q}| = N_Q \cdot K$ unlabeled (unseen) examples from each of the K classes. With models trained on the base set, few-shot techniques use the labeled support sets to adapt to the tasks at hand, and are evaluated based on their performances on the unlabeled query sets.

2.2 Proposed formulation

We begin by introducing some basic notation and definitions before presenting our overall Transductive Information Maximization (TIM) loss and the different optimization strategies for tackling it. For a given few-shot task with a support set \mathcal{S} and a query set \mathcal{Q} , let X denote the random variable associated with raw features within $\mathcal{S} \cup \mathcal{Q}$, and let $Y \in \mathcal{Y} = \{1, \dots, K\}$ be the random variable associated with labels. Let $f_\phi : \mathcal{X} \rightarrow \mathcal{Z}$ denote the encoder (*i.e.*, feature-extractor) function of a deep neural network, where ϕ denotes the trainable parameters, and \mathcal{Z} stands for the set of embedded features. The encoder is first trained from the base training set $\mathcal{X}_{\text{base}}$ using the standard cross-entropy loss without any meta training or specific sampling schemes. Then, for each specific few-shot task, we propose to minimize the mutual information loss defined over unlabeled query samples.

Formally, we define a soft-classifier whose posterior distribution over labels given features⁴ $p_{ik} := \mathbb{P}(Y = k | X = \mathbf{x}_i; \mathbf{W}, \phi)$ and marginal distribution over query labels $\hat{p}_k = \mathbb{P}(Y_{\mathcal{Q}} = k; \mathbf{W}, \phi)$ read:

$$p_{ik} \propto \exp\left(-\frac{\tau}{2} \|\mathbf{w}_k - \mathbf{z}_i\|^2\right), \quad \text{and} \quad \hat{p}_k = \frac{1}{|\mathcal{Q}|} \sum_{i \in \mathcal{Q}} p_{ik}, \quad (1)$$

where $\mathbf{W} := \{\mathbf{w}_1, \dots, \mathbf{w}_K\}$ denotes classifier weights, $\mathbf{z}_i = \frac{f_\phi(\mathbf{x}_i)}{\|f_\phi(\mathbf{x}_i)\|_2}$ the L2-normalized embedded features, and τ is a temperature parameter.

We can enunciate our empirical weighted mutual information between the query samples and their latent labels, which integrates two terms: The first is an empirical (Monte-Carlo) estimate of the conditional entropy of labels given query raw features $\hat{\mathcal{H}}(Y_{\mathcal{Q}} | X_{\mathcal{Q}})$ while the second is the empirical marginal label distribution $\hat{\mathcal{H}}(Y_{\mathcal{Q}})$:

$$\hat{\mathcal{I}}_\alpha(X_{\mathcal{Q}}; Y_{\mathcal{Q}}) := \underbrace{-\sum_{k=1}^K \hat{p}_k \log \hat{p}_k}_{\hat{\mathcal{H}}(Y_{\mathcal{Q}}): \text{marginal entropy}} + \alpha \underbrace{\frac{1}{|\mathcal{Q}|} \sum_{i \in \mathcal{Q}} \sum_{k=1}^K p_{ik} \log(p_{ik})}_{-\hat{\mathcal{H}}(Y_{\mathcal{Q}} | X_{\mathcal{Q}}): \text{conditional entropy}}, \quad (2)$$

with α a non-negative hyper-parameter. Notice that setting $\alpha = 1$ recovers the standard mutual information. Setting $\alpha < 1$ allows us to down-weight the conditional entropy term, whose gradients can erase the marginal entropy's gradients as the predictions move towards the vertices of the simplex. The role of both terms in (2) will be discussed after introducing a more general form of this loss.

In order to derive our overall Transductive Information Maximization (TIM) loss, we also need to embed supervision information from support set \mathcal{S} . This can be accomplished by integrating a standard cross-entropy loss CE with the information measure in Eq. (2):

$$\boxed{\mathcal{L}_{\text{TIM}} := \lambda \cdot \text{CE} - \hat{\mathcal{I}}_\alpha(X_{\mathcal{Q}}; Y_{\mathcal{Q}})} \quad \text{with} \quad \text{CE} := -\frac{1}{|\mathcal{S}|} \sum_{i \in \mathcal{S}} \sum_{k=1}^K y_{ik} \log(p_{ik}), \quad (3)$$

where $\{y_{ik}\}$ denotes the k^{th} component of the one-hot encoded label \mathbf{y}_i associated to the i -th support sample. Non-negative hyper-parameters α and λ will be fixed to $\alpha = \lambda = 0.1$ in all our experiments. Observe that by minimizing \mathcal{L}_{TIM} , we maximize the mutual information between the query inputs and corresponding latent labels, subject to support supervision constraints on predictions (posteriors). It is worth to discuss in more details the role (importance) of the mutual information terms in (3):

- Conditional entropy $\hat{\mathcal{H}}(Y_{\mathcal{Q}} | X_{\mathcal{Q}})$ aims at minimizing the uncertainty of the posteriors at unlabeled query samples, thereby encouraging the model to output *confident* predictions⁵. This entropy

⁴In order to simplify our notations, we deliberately omit the dependence of posteriors p_{ik} on the network parameters (ϕ, \mathbf{W}) , and p_{ik} takes the form of *softmax* predictions, but we omit the normalization constants.

⁵The global minima of each pointwise entropy in the sum of $\hat{\mathcal{H}}(Y_{\mathcal{Q}} | X_{\mathcal{Q}})$ are one-hot vectors at the vertices of the simplex.

loss is widely used in the context of semi-supervised learning (SSL) [9, 22, 1], as it models effectively the *cluster* assumption: The classifier’s boundaries should not occur at dense regions of the unlabeled features [9]. Recently, [5] introduced this term for few-shot learning, showing that entropy fine-tuning on query samples achieves competitive performances. In fact, if we remove the marginal entropy $\widehat{\mathcal{H}}(Y_{\mathcal{Q}})$ in objective (3), our TIM objective reduces to the loss in [5].

- The label-marginal entropy Marginal entropy regularizer $\widehat{\mathcal{H}}(Y_{\mathcal{Q}})$ is of high importance. As it will be observed from our experiments, it brings substantial improvements in performances (e.g., up to 10% increase in accuracy over entropy fine-tuning on the standard few-shot benchmarks), while facilitating optimization, thereby reducing transductive runtimes by several orders of magnitude. Worthwhile to mention that the conditional entropy $\widehat{\mathcal{H}}(Y_{\mathcal{Q}}|X_{\mathcal{Q}})$ is of paramount importance but its optimization requires special care, as its optima may easily lead to degenerate (non-suitable) solutions on the simplex vertices, mapping all samples to a single class. Such care may consist in using small learning rates and fine-tuning the whole network (which itself often contains several layers of regularization) as done in [5], both of which significantly slow down transductive inference. Marginal entropy regularizer $\widehat{\mathcal{H}}(Y_{\mathcal{Q}})$ encourages the marginal distribution of labels to be uniform, thereby avoiding such degenerate solutions. In particular, high-accuracy results can be obtained even using much higher learning rates and fine-tuning only a fraction of the network parameters (classifier weights \mathbf{W} instead of the whole network), speeding up substantially transductive runtimes (details in subsection 3.4).

2.3 Optimization

At this stage, we consider that the feature extractor has already been trained on base classes (using standard cross-entropy). We now propose two methods for minimizing our objective (3) for each test task. The first one is based on standard Gradient Descent (GD). The second is a novel way of optimizing mutual information, and is inspired by the Alternating Direction Method of Multipliers (ADMM). For both methods:

- The pre-trained feature extractor f_{ϕ} is kept fixed. Only the weights \mathbf{W} are adapted for each task. Such design choice is discussed in details in subsection 3.4. Overall, we found that fine-tuning only classifier weights \mathbf{W} yielded the best performances in terms of both accuracy and inference time.
- For each task, the weights \mathbf{W} are initialized as class prototypes computed from the support set:

$$\mathbf{w}_k^{(0)} = \left(\sum_{i \in \mathcal{S}} y_{ik} \mathbf{z}_i \right) / \left(\sum_{i \in \mathcal{S}} y_{ik} \right)$$

Gradient descent (TIM-GD): A straightforward way to minimize our loss in Eq. (3) is to perform gradient descent over the network parameters. Note that since our objective only depends on fixed extracted features $\{\mathbf{z}_i\}_{i \in \mathcal{S} \cup \mathcal{Q}}$, whose dimensions are lower than raw input images, we do not need mini-batch sampling: We can update the weights using all samples (from both support and query) at once. This gradient approach yields our overall best results, while being one order of magnitude faster than [5]. However, it still remains two orders of magnitude slower than inductive closed-form solutions [29]. In the following, we present a more efficient solver for our problem.

Alternating direction method (TIM-ADM): We derive an Alternating Direction Method (ADM) for minimizing our objective in (3). Such scheme yields substantial speedups in transductive learning (one order of magnitude) while maintaining similarly high levels of accuracy. To do so, we introduce auxiliary variables representing latent assignments of query samples, and minimize a mixed-variable objective by alternating two sub-steps, one optimizing w.r.t classifier’s weights \mathbf{W} , and the other w.r.t the auxiliary variables \mathbf{q} .

Proposition 1. *The objective in (3) can be approximately minimized via the following constrained formulation of the optimization problem:*

$$\begin{aligned} \min_{\mathbf{W}, \mathbf{q}} & \underbrace{-\frac{\lambda}{|\mathcal{S}|} \sum_{i \in \mathcal{S}} \sum_{k=1}^K y_{ik} \log(p_{ik})}_{\text{CE}} + \underbrace{\sum_{k=1}^K \hat{q}_k \log \frac{\hat{q}_k}{\pi_k}}_{\sim \hat{\mathcal{H}}(Y_{\mathcal{Q}})} - \underbrace{\frac{\alpha}{|\mathcal{Q}|} \sum_{i \in \mathcal{Q}} \sum_{k=1}^K q_{ik} \log(p_{ik})}_{\sim \hat{\mathcal{H}}(Y_{\mathcal{Q}}|X_{\mathcal{Q}})} + \underbrace{\frac{1}{|\mathcal{Q}|} \sum_{i \in \mathcal{Q}} \sum_{k=1}^K q_{ik} \log \frac{q_{ik}}{p_{ik}}}_{\text{Penalty} \equiv \mathcal{D}_{\text{KL}}(\mathbf{q} \parallel \mathbf{p})} \\ \text{s.t.} & \sum_{k=1}^K q_{ik} = 1, \quad q_{ik} \geq 0, \quad i \in \mathcal{Q}, \quad k \in \{1, \dots, K\}, \end{aligned} \quad (4)$$

where $\mathbf{q} = [q_{ik}] \in \mathbb{R}^{|\mathcal{Q}| \times K}$ are auxiliary variables, $\mathbf{p} = [p_{ik}] \in \mathbb{R}^{|\mathcal{Q}| \times K}$ and $\hat{q}_k = \frac{1}{|\mathcal{Q}|} \sum_{i \in \mathcal{Q}} q_{ik}$.

Proof. It is straightforward to notice that, when equality constraints $q_{ik} = p_{ik}$ are satisfied, the last term in objective (4), which can be viewed as a soft penalty for enforcing those equality constraints, vanishes. Objectives (3) and (4) then become equivalent. \square

Splitting the problem into sub-problems on \mathbf{W} and \mathbf{q} as in Eq. (4) is closely related to the general principle of ADMM (Alternating Direction Method of Multipliers) [2], except that the KL divergence is not a typical penalty for imposing the equality constraints.⁶ The main idea is to **decompose the original problem into two easier sub-problems**, one over \mathbf{W} and the other over \mathbf{q} , which can alternately be solved in closed-form. Interestingly, this KL penalty is important as it completely removes the need for dual iterations for the simplex constraints in (4), yielding closed-form solutions:

Proposition 2. *ADM formulation in Proposition 1 can be approximately solved by alternating the following closed-form updates w.r.t auxiliary variables \mathbf{q} and classifier weights \mathbf{W} (t is the iteration index):*

$$q_{ik}^{(t+1)} \propto \frac{(p_{ik}^{(t)})^{1+\alpha}}{\left(\sum_{i \in \mathcal{Q}} (p_{ik}^{(t)})^{1+\alpha}\right)^{1/2}} \quad (5)$$

$$\mathbf{w}_k^{(t+1)} \leftarrow \frac{\frac{\lambda}{1+\alpha} \left[\sum_{i \in \mathcal{S}} y_{ik} \mathbf{z}_i + p_{ik}^{(t)} (\mathbf{w}_k^{(t)} - \mathbf{z}_i) \right] + \frac{|\mathcal{S}|}{|\mathcal{Q}|} \left[\sum_{i \in \mathcal{Q}} q_{ik}^{(t+1)} \mathbf{z}_i + p_{ik}^{(t)} (\mathbf{w}_k^{(t)} - \mathbf{z}_i) \right]}{\frac{\lambda}{1+\alpha} \sum_{i \in \mathcal{S}} y_{ik} + \frac{|\mathcal{S}|}{|\mathcal{Q}|} \sum_{i \in \mathcal{Q}} q_{ik}^{(t+1)}} \quad (6)$$

Proof. A detailed proof is deferred to the supplemental material. Here, we summarize the main technical ingredients of the approximation. Keeping the auxiliary variables \mathbf{q} fixed, we optimize a convex approximation w.r.t \mathbf{W} , obtained after decomposing Eq. (4) and linearizing the non-convex part. With \mathbf{W} fixed, the objective is strictly convex w.r.t the auxiliary variables \mathbf{q} whose updates come from a closed-form solution of the KKT (Karush–Kuhn–Tucker) conditions. Interestingly, the negative entropy of auxiliary variables, which appears in the penalty term, handles implicitly the simplex constraints, which removes the need for dual iterations to solve the KKT conditions. \square

We will refer to this approach as *TIM-ADM*. The detailed algorithms for TIM-GD and TIM-ADM are presented in Appendix A.

3 Experiments

Hyperparameters: To keep our experiments as simple as possible, **our hyperparameters are kept fixed across all the experiments and methods (TIM-GD and TIM-ADM)**. The conditional entropy weight α and the cross-entropy weights λ in Objective (3) are both set to 0.1. The temperature parameter τ in the classifier is set to 15. In our TIM-GD method, we use the ADAM optimizer with

⁶Typically, ADMM methods use multiplier-based quadratic penalties for enforcing the equality constraint.

the recommended parameters [15], and run 1000 iterations for each task. For TIM-ADM, we run 150 iterations.

Training procedure: Base-class training of our feature extractor follows the same protocol as in [42] for all the experiments. As mentioned in subsection 2.2, it follows the standard form of cross-entropy training, without meta-learning schemes. The detailed procedure can be found in [42]. We summarize it thereafter: SGD optimizer is used to train the models, with mini-batch size set to 256 for ResNet-18 and 128 for WRN28-10. Label smoothing [32] with a fixed smoothing parameter $\epsilon = 0.1$, as well as color jittering similar to [3, 5] is used.

Datasets: We resort to 3 few-shot learning datasets to benchmark the proposed models. As standard few-shot benchmarks, we use the *mini-Imagenet* [36], with 100 classes split as in [26], as well as the larger *tiered-Imagenet* dataset, with 608 classes split as in [27]. To evaluate our method under large domain-shift, we use the *Caltech-UCSD Birds 200* [38] (CUB), which contains 200 classes, split following [3].

3.1 Comparison to state-of-the-art

We first evaluate our methods TIM-GD and TIM-ADM on the widely adopted *mini-ImageNet*, *tiered-ImageNet* and *CUB* benchmark datasets, in the most common 1-shot 5-way and 5-shot 5-way scenarios, with 15 query shots for each class. Results are reported in Table 1, and are averaged over 10,000 episodes, following [37]. We can observe that both TIM-GD and TIM-ADM exhibit state-of-the-art performances, consistently across datasets, scenarios and backbones, improving over both transductive and inductive methods, by significant margins.

3.2 Impact of domain-shift

Chen et al. [3] recently showed that the performance of most meta-learning methods may drop drastically when a domain-shift exists between the base training data and test data. Surprisingly, the simplest discriminative baseline exhibited the best performance in this case. Therefore, we evaluate our methods in this challenging scenario. To this end, we simulate a domain shift by training the feature encoder on *mini-ImageNet* while evaluating the methods on *CUB*. TIM-GD and TIM-ADM beat previous methods by significant margin in the domain shift scenario, consistently with our results in the standard few-shot benchmarks, thereby demonstrating an increased potential of applicability to real-world situations.

3.3 Pushing the meta-testing stage

Most few-shot papers only evaluate their method in the usual 5-way scenario. Nevertheless, [3] showed that meta-learning methods could be beaten by their discriminative baseline when more ways were introduced in each task. Therefore, we also provide results of our method in the more challenging 10-way and 20-way scenarios on *mini-ImageNet*. These results, which are presented in Table 3, show that TIM-GD outperforms other methods by a significant margin in both settings.

3.4 Ablation study

Influence of each term: We now assess the impact of each term in our loss in Eq. (3)⁷ on the final performance of our methods. The results are reported in Table 4. We observe that the integration of the three terms in our loss consistently outperforms any other configuration. Interestingly, the absence of the marginal entropy $\hat{\mathcal{H}}(Y_{\mathcal{Q}})$ in both TIM-GD and TIM-ADM (referred to as TIM-GD $\{\mathbf{W}\}$ and TIM-ADM $\{\mathbf{W}\}$) leads to poor performances. Such behavior results from the conditional entropy term yielding degenerate solutions (assigning all query samples to a single class) on numerous tasks, and emphasizes the importance of the marginal entropy term $\hat{\mathcal{H}}(Y_{\mathcal{Q}})$ in our loss (3), that acts as a powerful regularizer to prevent such trivial solutions.

Fine-tuning the whole network vs only the classifier weights: While our TIM-GD and TIM-ADM optimize w.r.t \mathbf{W} and keep base-trained encoder f_{ϕ} fixed at inference, the authors of [5] fine-tuned the whole network $\{\mathbf{W}, \phi\}$ when performing their transductive entropy minimization. To assess both

⁷The \mathbf{W} and \mathbf{q} updates of TIM-ADM associated to each configuration can be found in supp. material.

Table 1: Comparison to the state-of-the-art methods on *mini-ImageNet* and *tiered-Imagenet*. The methods are sub-grouped into transductive and inductive methods, as well as by backbone architecture. Our results (gray-shaded) are averaged over 10,000 episodes. "-" signifies the result is unavailable.

Method	Transductive	Backbone	<i>mini-ImageNet</i>		<i>tiered-ImageNet</i>		CUB	
			1-shot	5-shot	1-shot	5-shot	1-shot	5-shot
MAML [7]		ResNet-18	49.6	65.7	-	-	68.4	83.5
RelatNet [31]		ResNet-18	52.5	69.8	-	-	68.6	84.0
MatchNet [36]		ResNet-18	52.9	68.9	-	-	73.5	84.5
ProtoNet [29]		ResNet-18	54.2	73.4	-	-	73.0	86.6
MTL [30]	✗	ResNet-12	61.2	75.5	-	-	-	-
vFSL [41]		ResNet-12	61.2	77.7	-	-	-	-
Neg-cosine [17]		ResNet-18	62.3	80.9	-	-	72.7	89.4
MetaOpt [16]		ResNet-12	62.6	78.6	66.0	81.6	-	-
SimpleShot [37]		ResNet-18	62.9	80.0	68.9	84.6	68.9	84.0
Distill [33]		ResNet-12	64.8	82.1	71.5	86.0	-	-
RelatNet + T [11]		ResNet-12	52.4	65.4	-	-	-	-
ProtoNet + T [11]		ResNet-12	55.2	71.1	-	-	-	-
MatchNet+T [11]		ResNet-12	56.3	69.8	-	-	-	-
TPN [19]		ResNet-12	59.5	75.7	-	-	-	-
TEAM [25]		ResNet-18	60.1	75.9	-	-	-	-
Ent-min [5]	✓	ResNet-12	62.4	74.5	68.4	83.4	-	-
CAN+T [11]		ResNet-12	67.2	80.6	73.2	84.9	-	-
LaplacianShot [42]		ResNet-18	72.1	82.3	79.0	86.4	81.0	88.7
TIM-ADM		ResNet-18	73.6	85.0	80.0	88.5	81.9	90.7
TIM-GD		ResNet-18	73.9	85.0	79.9	88.5	82.2	90.8
LEO [28]		WRN28-10	61.8	77.6	66.3	81.4	-	-
SimpleShot [37]		WRN28-10	63.5	80.3	69.8	85.3	-	-
MatchNet [36]	✗	WRN28-10	64.0	76.3	-	-	-	-
CC+rot+unlabeled [8]		WRN28-10	64.0	80.7	70.5	85.0	-	-
FEAT [40]		WRN28-10	65.1	81.1	70.4	84.4	-	-
AWGIM [10]		WRN28-10	63.1	78.4	67.7	82.8	-	-
Ent-min [5]		WRN28-10	65.7	78.4	73.3	85.5	-	-
SIB [12]		WRN28-10	70.0	79.2	-	-	-	-
BD-CSPN [18]	✓	WRN28-10	70.3	81.9	78.7	86.92	-	-
LaplacianShot [42]		WRN28-10	74.9	84.1	80.2	87.6	-	-
TIM-ADM		WRN28-10	77.5	87.2	82.0	89.7	-	-
TIM-GD		WRN28-10	77.8	87.4	82.1	89.8	-	-

Table 2: Results for CUB and domain-shift *mini-Imagenet* \rightarrow CUB. Results obtained by our models (gray-shaded) are averaged over 10,000 episodes.

Methods	Backbone	<i>mini-ImageNet</i> \rightarrow CUB
		5-shot
MatchNet [36]	ResNet-18	53.1
MAML [7]	ResNet-18	51.3
ProtoNet [29]	ResNet-18	62.0
RelatNet [31]	ResNet-18	57.7
SimpleShot [37]	ResNet-18	64.0
GNN [34]	ResNet-10	66.9
Neg-Cosine [17]	ResNet-18	67.0
Baseline [3]	ResNet-18	65.6
LaplacianShot [42]	ResNet-18	66.3
TIM-ADM	ResNet-18	70.3
TIM-GD	ResNet-18	71.0

Table 3: Results for increasing ways on *mini*-ImageNet. Results obtained by our models (gray-shaded) are averaged over 10,000 episodes.

Methods	Backbone	10-way		20-way	
		1-shot	5-shot	1-shot	5-shot
MatchNet [36]	ResNet-18	-	52.3	-	36.8
ProtoNet [29]	ResNet-18	-	59.2	-	45.0
RelatNet [31]	ResNet-18	-	53.9	-	39.2
SimpleShot [37]	ResNet-18	45.1	68.1	32.4	55.4
Baseline [3]	ResNet-18	-	55.0	-	42.0
Baseline++ [3]	ResNet-18	-	63.4	-	50.9
TIM-ADM	ResNet-18	56.0	72.9	39.5	58.8
TIM-GD	ResNet-18	56.1	72.8	39.3	59.5

Table 4: Ablation study on the effect of each term in the loss on balanced tasks, when only the prototypes are finetuned ($\{\mathbf{W}\}$) and when the whole network is finetuned ($\{\phi, \mathbf{W}\}$). Results reported for TIM-GD are based on the model employing ResNet-18 as backbone. The same term indexing as in Eq. (3) are used here: $\hat{\mathcal{H}}(Y_{\mathcal{Q}})$: Marginal entropy, $\hat{\mathcal{H}}(Y_{\mathcal{Q}}|X_{\mathcal{Q}})$: Conditional entropy, CE: Cross-entropy.

Method	Parameters	Loss	<i>mini</i> -ImageNet		<i>tiered</i> -ImageNet		CUB	
			1-shot	5-shot	1-shot	5-shot	1-shot	5-shot
TIM-ADM	$\{\mathbf{W}\}$	CE	60.0	79.6	68.0	84.6	68.6	86.4
		CE + $\hat{\mathcal{H}}(Y_{\mathcal{Q}} X_{\mathcal{Q}})$	36.0	77.0	48.1	82.5	48.5	86.5
		CE - $\hat{\mathcal{H}}(Y_{\mathcal{Q}})$	66.7	82.0	74.0	86.5	74.2	88.3
		CE - $\hat{\mathcal{H}}(Y_{\mathcal{Q}})$ + $\hat{\mathcal{H}}(Y_{\mathcal{Q}} X_{\mathcal{Q}})$	73.6	85.0	80.0	88.5	81.9	90.7
TIM-GD	$\{\mathbf{W}\}$	CE	60.7	79.4	68.4	84.3	69.6	86.3
		CE + $\hat{\mathcal{H}}(Y_{\mathcal{Q}} X_{\mathcal{Q}})$	35.3	79.2	45.9	80.6	46.1	85.9
		CE - $\hat{\mathcal{H}}(Y_{\mathcal{Q}})$	66.1	81.3	73.4	86.0	73.9	88.0
		CE - $\hat{\mathcal{H}}(Y_{\mathcal{Q}})$ + $\hat{\mathcal{H}}(Y_{\mathcal{Q}} X_{\mathcal{Q}})$	73.9	85.0	79.9	88.5	82.2	90.8
TIM-GD	$\{\phi, \mathbf{W}\}$	CE	60.8	81.6	65.7	83.5	68.7	87.7
		CE + $\hat{\mathcal{H}}(Y_{\mathcal{Q}} X_{\mathcal{Q}})$	62.7	81.9	66.9	82.8	72.6	89.0
		CE - $\hat{\mathcal{H}}(Y_{\mathcal{Q}})$	62.3	82.7	68.3	85.4	70.7	88.8
		CE - $\hat{\mathcal{H}}(Y_{\mathcal{Q}})$ + $\hat{\mathcal{H}}(Y_{\mathcal{Q}} X_{\mathcal{Q}})$	67.2	84.7	73.0	86.8	76.7	90.5

approaches, we add to Table 4 a variant of TIM-GD, in which we fine-tune the whole network $\{\mathbf{W}, \phi\}$, by using the same optimization procedure as in [5]. We found that, besides being much slower, fine-tuning the whole network with \mathcal{L}_{TIM} degrades the performances, as also conveyed by the convergence plots in Figure 1. Such results validate our initial optimization choice. Interestingly, when fine-tuning the whole network $\{\mathbf{W}, \phi\}$, the absence of $\hat{\mathcal{H}}(Y_{\mathcal{Q}})$ in the entropy-based loss CE + $\hat{\mathcal{H}}(Y_{\mathcal{Q}}|X_{\mathcal{Q}})$ does not cause the same drastic drop in performance as observed earlier when optimizing only w.r.t \mathbf{W} . We hypothesize that the network’s intrinsic regularization (such as batch normalizations) and the use of small learning rates, as prescribed by [5], help the optimization process, preventing the predictions from approaching the vertices of the simplex, where entropy’s gradients diverge.

3.5 Computational complexity

Transductive methods are generally slower at inference than their inductive counterparts, with runtimes spanning multiple orders of magnitude across methods. In Table 5, we measure the average adaptation time, defined as the time required by each method to build the final classifier, for a 5-shot 5-way task on *mini*-ImageNet using a WRN28-10 network. Table 5 conveys that our ADM optimization allows to gain one order of magnitude in runtime over our gradient-based method, and more than two orders of magnitude in comparison to [5] that finetunes the whole network. Note that TIM-ADM still remains slower than the inductive baseline, and [42]. Our methods were run on the same GTX 1080 Ti GPU, while [5] and [42] were directly reported from the papers.

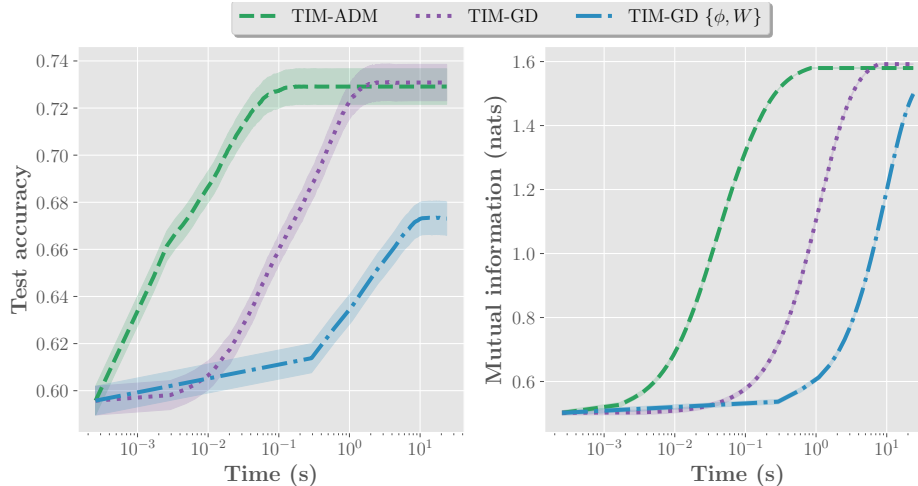


Figure 1: Convergence plots for our methods on *mini-ImageNet* with a ResNet-18. Solid lines are averages, while shadows are 95% confidence intervals. Time is in logarithmic scale. **Left:** Evolution of the test accuracy during transductive inference. **Right:** Evolution of the mutual information between query features and predictions $\hat{\mathcal{I}}(X_Q; Y_Q)$, computed as in Eq. (2) (with $\alpha = 1$).

Table 5: Inference runtime per task for a 5-shot 5-way task on *mini-ImageNet* with a WRN28-10 backbone.

Runtimes			
Method	Param.	Transd.	Inference/task (s)
SimpleShot [37]	$\{\mathbf{W}\}$	\times	$9.0 e^{-3}$
LaplacianShot	$\{\mathbf{W}\}$		$1.2 e^{-2}$
TIM-ADM	$\{\mathbf{W}\}$		$1.2 e^{-1}$
TIM-GD	$\{\mathbf{W}\}$	\checkmark	$2.2 e^{+0}$
Ent-min [5]	$\{\phi, \mathbf{W}\}$		$2.1 e^{+1}$

4 Conclusion and future work

We establish new state-of-the-art results on the standard few-shot benchmarks, as well as in difficult scenarios with more ways or domain shift, using our transductive information maximization objective. In future work, we target on giving a more theoretical ground for our proposed objective. Specifically, our goal will be to connect the TIM objective to our classifier’s empirical risk on the query set, showing that the former could be viewed as a surrogate for the latter.

References

- [1] David Berthelot, Nicholas Carlini, Ian Goodfellow, Nicolas Papernot, Avital Oliver, and Colin A Raffel. Mixmatch: A holistic approach to semi-supervised learning. In *Advances in Neural Information Processing Systems (NeurIPS)*, 2019.
- [2] Stephen Boyd, Neal Parikh, Eric Chu, Borja Peleato, and Jonathan Eckstein. Distributed optimization and statistical learning via the alternating direction method of multipliers. In *Foundations and Trends® in Machine learning*. Now Publishers Inc., 2011.
- [3] Wei-Yu Chen, Yen-Cheng Liu, Zsolt Kira, Yu-Chiang Frank Wang, and Jia-Bin Huang. A closer look at few-shot classification. In *International Conference on Learning Representations (ICLR)*, 2019.
- [4] Zhou Dengyong, Olivier Bousquet, Thomas N Lal, Jason Weston, and Bernhard Schölkopf. Learning with local and global consistency. In *Advances in neural information processing systems (NeurIPS)*, 2004.
- [5] Guneet S Dhillon, Pratik Chaudhari, Avinash Ravichandran, and Stefano Soatto. A baseline for few-shot image classification. In *International Conference on Learning Representations (ICLR)*, 2020.
- [6] Li Fei-Fei, Rob Fergus, and Pietro Perona. One-shot learning of object categories. In *IEEE transactions on pattern analysis and machine intelligence (PAMI)*. IEEE, 2006.
- [7] Chelsea Finn, Pieter Abbeel, and Sergey Levine. Model-agnostic meta-learning for fast adaptation of deep networks. In *Proceedings of the 34th International Conference on Machine Learning (ICML)*, 2017.
- [8] Spyros Gidaris, Andrei Bursuc, Nikos Komodakis, Patrick Pérez, and Matthieu Cord. Boosting few-shot visual learning with self-supervision. In *Proceedings of the IEEE International Conference on Computer Vision (ICCV)*, 2019.
- [9] Yves Grandvalet and Yoshua Bengio. Semi-supervised learning by entropy minimization. In *Advances in neural information processing systems (NeurIPS)*, 2005.
- [10] Yiluan Guo and Ngai-Man Cheung. Attentive weights generation for few shot learning via information maximization. In *Proceedings of the IEEE/CVF Conference on Computer Vision and Pattern Recognition (CVPR)*, 2020.
- [11] Ruibing Hou, Hong Chang, MA Bingpeng, Shiguang Shan, and Xilin Chen. Cross attention network for few-shot classification. In *Advances in Neural Information Processing Systems (NeurIPS)*, 2019.
- [12] Shell Xu Hu, Pablo G Moreno, Yang Xiao, Xi Shen, Guillaume Obozinski, Neil D Lawrence, and Andreas Damianou. Empirical bayes transductive meta-learning with synthetic gradients. In *International Conference on Learning Representations (ICLR)*, 2020.
- [13] Thorsten Joachims. Transductive inference for text classification using support vector machines. In *Proceedings of the Sixteenth International Conference on Machine Learning (ICML)*. Morgan Kaufmann Publishers Inc., 1999.
- [14] Jongmin Kim, Taesup Kim, Sungwoong Kim, and Chang D Yoo. Edge-labeling graph neural network for few-shot learning. In *Proceedings of the IEEE Conference on Computer Vision and Pattern Recognition (CVPR)*, 2019.
- [15] Diederik P. Kingma and Jimmy Ba. Adam: A method for stochastic optimization. In *International Conference on Learning Representations (ICLR)*, 2014.
- [16] Kwonjoon Lee, Subhransu Maji, Avinash Ravichandran, and Stefano Soatto. Meta-learning with differentiable convex optimization. In *Proceedings of the IEEE Conference on Computer Vision and Pattern Recognition (CVPR)*, 2019.
- [17] Bin Liu, Yue Cao, Yutong Lin, Qi Li, Zheng Zhang, Mingsheng Long, and Han Hu. Negative margin matters: Understanding margin in few-shot classification. In *European Conference on Computer Vision (ECCV)*, 2020.
- [18] Jinlu Liu, Liang Song, and Yongqiang Qin. Prototype rectification for few-shot learning. In *European Conference on Computer Vision (ECCV)*, 2020.

- [19] Yanbin Liu, Juho Lee, Minseop Park, Saehoon Kim, Eunho Yang, Sung Ju Hwang, and Yi Yang. Learning to propagate labels: Transductive propagation network for few-shot learning. In *International Conference on Learning Representations (ICLR)*, 2019.
- [20] Erik G Miller, Nicholas E Matsakis, and Paul A Viola. Learning from one example through shared densities on transforms. In *Proceedings IEEE Conference on Computer Vision and Pattern Recognition (CVPR)*, 2000.
- [21] N. Mishra, M. Rohaninejad, X. Chen, and P. A. Abbeel. simple neural attentive meta-learner. In *International Conference on Learning Representations (ICLR)*, 2018.
- [22] Takeru Miyato, Shin-ichi Maeda, Masanori Koyama, and Shin Ishii. Virtual adversarial training: a regularization method for supervised and semi-supervised learning. In *IEEE transactions on pattern analysis and machine intelligence (PAMI)*, 2018.
- [23] Alex Nichol, Joshua Achiam, and John Schulman. On first-order meta-learning algorithms, 2018.
- [24] Boris Oreshkin, Pau Rodríguez López, and Alexandre Lacoste. Tadam: Task dependent adaptive metric for improved few-shot learning. In *Advances in Neural Information Processing Systems (NeurIPS)*, 2018.
- [25] Limeng Qiao, Yemin Shi, Jia Li, Yaowei Wang, Tiejun Huang, and Yonghong Tian. Transductive episodic-wise adaptive metric for few-shot learning. In *Proceedings of the IEEE International Conference on Computer Vision (ICCV)*, 2019.
- [26] Sachin Ravi and Hugo Larochelle. Optimization as a model for few-shot learning. In *International Conference on Learning Representations (ICLR)*, 2016.
- [27] Mengye Ren, Eleni Triantafillou, Sachin Ravi, Jake Snell, Kevin Swersky, Joshua B Tenenbaum, Hugo Larochelle, and Richard S Zemel. Meta-learning for semi-supervised few-shot classification. In *International Conference on Learning Representations (ICLR)*, 2018.
- [28] Andrei A Rusu, Dushyant Rao, Jakub Sygnowski, Oriol Vinyals, Razvan Pascanu, Simon Osindero, and Raia Hadsell. Meta-learning with latent embedding optimization. In *International Conference on Learning Representations (ICLR)*, 2019.
- [29] Jake Snell, Kevin Swersky, and Richard Zemel. Prototypical networks for few-shot learning. In *Advances in neural information processing systems (NeurIPS)*, 2017.
- [30] Qianru Sun, Yaoyao Liu, Tat-Seng Chua, and Bernt Schiele. Meta-transfer learning for few-shot learning. In *Proceedings of the IEEE Conference on Computer Vision and Pattern Recognition (CVPR)*, 2019.
- [31] Flood Sung, Yongxin Yang, Li Zhang, Tao Xiang, Philip HS Torr, and Timothy M Hospedales. Learning to compare: Relation network for few-shot learning. In *Proceedings of the IEEE Conference on Computer Vision and Pattern Recognition (CVPR)*, 2018.
- [32] Christian Szegedy, Vincent Vanhoucke, Sergey Ioffe, Jon Shlens, and Zbigniew Wojna. Rethinking the inception architecture for computer vision. In *Conference on computer vision and pattern recognition (CVPR)*, 2016.
- [33] Yonglong Tian, Yue Wang, Dilip Krishnan, Joshua B. Tenenbaum, and Phillip Isola. Rethinking few-shot image classification: a good embedding is all you need? In *European Conference on Computer Vision (ECCV)*, 2020.
- [34] Hung-Yu Tseng, Hsin-Ying Lee, Jia-Bin Huang, and Ming-Hsuan Yang. Cross-domain few-shot classification via learned feature-wise transformation. In *International Conference on Learning Representations (ICLR)*, 2020.
- [35] Vladimir N Vapnik. An overview of statistical learning theory. In *IEEE transactions on neural networks*. IEEE, 1999.
- [36] Oriol Vinyals, Charles Blundell, Timothy Lillicrap, Daan Wierstra, et al. Matching networks for one shot learning. In *Advances in neural information processing systems (NeurIPS)*, 2016.
- [37] Yan Wang, Wei-Lun Chao, Kilian Q Weinberger, and Laurens van der Maaten. Simpleshot: Revisiting nearest-neighbor classification for few-shot learning. In *arXiv preprint arXiv:1911.04623*, 2019.
- [38] P. Welinder, S. Branson, T. Mita, C. Wah, F. Schroff, S. Belongie, and P. Perona. Caltech-UCSD Birds 200. Technical Report CNS-TR-2010-001, California Institute of Technology, 2010.

- [39] Davis Wertheimer and Bharath Hariharan. Few-shot learning with localization in realistic settings. In *Proceedings of the IEEE Conference on Computer Vision and Pattern Recognition (CVPR)*, 2019.
- [40] Han-Jia Ye, Hexiang Hu, De-Chuan Zhan, and Fei Sha. Learning embedding adaptation for few-shot learning. In *Conference on Computer Vision and Pattern Recognition (CVPR)*, 2020.
- [41] Jian Zhang, Chenglong Zhao, Bingbing Ni, Minghao Xu, and Xiaokang Yang. Variational few-shot learning. In *The IEEE International Conference on Computer Vision (ICCV)*, October 2019.
- [42] Imtiaz Masud Ziko, Jose Dolz, Eric Granger, and Ismail Ben Ayed. Laplacian regularized few-shot learning. In *International Conference on Machine Learning (ICML)*, 2020.

A Algorithms

Algorithm 1: TIM-ADM

Input : Pretrained encoder f_ϕ , Task $\{\mathcal{S}, \mathcal{Q}\}$, # iterations $iter$, Temperature τ , Weights $\{\lambda, \alpha\}$

$$\mathbf{z}_i \leftarrow f_\phi(\mathbf{x}_i) / \|f_\phi(\mathbf{x}_i)\|_2, i \in \mathcal{S} \cup \mathcal{Q}$$

$$\mathbf{w}_k \leftarrow \sum_{i \in \mathcal{S}} y_{ik} \mathbf{z}_i / \sum_{i \in \mathcal{S}} y_{ik}, k \in \{1, \dots, K\}$$

for $i \leftarrow 0$ **to** $iter$ **do**

$$p_{ik} \leftarrow \exp\left(-\frac{\tau}{2} \|\mathbf{w}_k - \mathbf{z}_i\|^2\right), i \in \mathcal{S} \cup \mathcal{Q}$$

$$p_{ik} \leftarrow p_{ik} / \sum_{l=1}^K p_{il}$$

$$q_{ik} \leftarrow p_{ik}^{1+\alpha} / \left(\sum_{i \in \mathcal{Q}} p_{ik}^{1+\alpha}\right)^{1/2}, i \in \mathcal{Q}$$

$$q_{ik} \leftarrow q_{ik} / \sum_{l=1}^K q_{il}$$

$$\mathbf{w}_k \leftarrow \frac{\frac{\lambda}{1+\alpha} \left[\sum_{i \in \mathcal{S}} y_{ik} \mathbf{z}_i + p_{ik}(\mathbf{w}_k - \mathbf{z}_i) \right] + \frac{|\mathcal{S}|}{|\mathcal{Q}|} \left[\sum_{i \in \mathcal{Q}} q_{ik} \mathbf{z}_i + p_{ik}(\mathbf{w}_k - \mathbf{z}_i) \right]}{\frac{\lambda}{1+\alpha} \sum_{i \in \mathcal{S}} y_{ik} + \frac{|\mathcal{S}|}{|\mathcal{Q}|} \sum_{i \in \mathcal{Q}} q_{ik}}$$

end

Result: Query predictions $\hat{y}_i = \arg \max_k p_{ik}, i \in \mathcal{Q}$

Algorithm 2: TIM-GD

Input : Pretrained encoder f_ϕ , Task $\{\mathcal{S}, \mathcal{Q}\}$, # iterations $iter$, Temperature τ , Weights $\{\lambda, \alpha\}$,
Learning rate γ

$$\mathbf{z}_i \leftarrow f_\phi(\mathbf{x}_i) / \|f_\phi(\mathbf{x}_i)\|_2, i \in \mathcal{S} \cup \mathcal{Q}$$

$$\mathbf{w}_k \leftarrow \sum_{i \in \mathcal{S}} y_{ik} \mathbf{z}_i / \sum_{i \in \mathcal{S}} y_{ik}, k \in \{1, \dots, K\}$$

for $i \leftarrow 0$ **to** $iter$ **do**

$$p_{ik} \leftarrow \exp\left(-\frac{\tau}{2} \|\mathbf{w}_k - \mathbf{z}_i\|^2\right)$$

$$p_{ik} \leftarrow p_{ik} / \sum_{l=1}^K p_{il}$$

$$\mathbf{w}_k \leftarrow \mathbf{w}_k - \gamma \nabla_{\mathbf{w}_k} \mathcal{L}_{\text{TIM}}$$

end

Result: Query predictions $\hat{y}_i = \arg \max_k p_{ik}, i \in \mathcal{Q}$

B Proofs

Proof of Proposition 1

Proof. Let us start from the initial optimization problem:

$$\min_{\mathbf{w}} \sum_{k=1}^K \hat{p}_k \log \hat{p}_k - \frac{\alpha}{|\mathcal{Q}|} \sum_{i \in \mathcal{Q}} \sum_{k=1}^K p_{ik} \log p_{ik} - \frac{\lambda}{|\mathcal{S}|} \sum_{i \in \mathcal{S}} \sum_{k=1}^K y_{ik} \log p_{ik} \quad (7)$$

We can reformulate problem (7) using the ADM approach, i.e., by introducing auxiliary variables $\mathbf{q} = [q_{ik}] \in \mathbb{R}^{|\mathcal{Q}| \times K}$ and enforcing equality constraint $\mathbf{q} = \mathbf{p}$, with $\mathbf{p} = [p_{ik}] \in \mathbb{R}^{|\mathcal{Q}| \times K}$, in addition

to pointwise simplex constraints:

$$\begin{aligned}
\min_{\mathbf{W}, \mathbf{q}} \quad & \sum_{k=1}^K \hat{q}_k \log \hat{q}_k - \frac{\alpha}{|\mathcal{Q}|} \sum_{i \in \mathcal{Q}} \sum_{k=1}^K q_{ik} \log p_{ik} - \frac{\lambda}{|\mathcal{S}|} \sum_{i \in \mathcal{S}} \sum_{k=1}^K y_{ik} \log p_{ik} \quad (8) \\
\text{s.t.} \quad & q_{ik} = p_{ik}, \quad i \in \mathcal{Q}, \quad k \in \{1, \dots, K\} \\
& \sum_{k=1}^K q_{ik} = 1, \quad i \in \mathcal{Q} \\
& q_{ik} \geq 0, \quad i \in \mathcal{Q}, \quad k \in \{1, \dots, K\} \quad (9)
\end{aligned}$$

We can solve constrained problem (8) with a penalty-based approach, which encourages auxiliary pointwise predictions $\mathbf{q}_i = [q_{i1}, \dots, q_{iK}]$ to be close to our model's posteriors $\mathbf{p}_i = [p_{i1}, \dots, p_{iK}]$. We use the KL divergence for this penalty:

$$\begin{aligned}
\min_{\mathbf{W}, \mathbf{q}} \quad & \sum_{k=1}^K \hat{q}_k \log \hat{q}_k - \frac{\alpha}{|\mathcal{Q}|} \sum_{i \in \mathcal{Q}} \sum_{k=1}^K q_{ik} \log p_{ik} - \frac{\lambda}{|\mathcal{S}|} \sum_{i \in \mathcal{S}} \sum_{k=1}^K y_{ik} \log p_{ik} + \frac{1}{|\mathcal{Q}|} \sum_{i \in \mathcal{Q}} \mathcal{D}_{\text{KL}}(\mathbf{q}_i \| \mathbf{p}_i) \\
\text{s.t.} \quad & \sum_{k=1}^K q_{ik} = 1, \quad i \in \mathcal{Q} \quad (10) \\
& q_{ik} \geq 0, \quad i \in \mathcal{Q}, \quad k \in \{1, \dots, K\}
\end{aligned}$$

□

Proof of Proposition 2

Proof. Recall that we consider a softmax classifier over distances to weights $\mathbf{W} = \{\mathbf{w}_1, \dots, \mathbf{w}_K\}$. To simplify the notations, we will omit the dependence upon ϕ in what follows, and write $\mathbf{z}_i = \frac{f_\phi(\mathbf{x}_i)}{\|f_\phi(\mathbf{x}_i)\|}$ such that $p_{ik} \propto e^{-\frac{\tau}{2} \|\mathbf{z}_i - \mathbf{w}_k\|^2}$. With loss of generality, we implicitly used $\tau = 1$. After plugging in the expression of p_{ik} into Eq. (4) and grouping terms together, we get:

$$\begin{aligned}
(4) &= \sum_{k=1}^K \hat{q}_k \log \hat{q}_k - \frac{1 + \alpha}{|\mathcal{Q}|} \sum_{i \in \mathcal{Q}} \sum_{k=1}^K q_{ik} \log p_{ik} - \frac{\lambda}{|\mathcal{S}|} \sum_{i \in \mathcal{S}} \sum_{k=1}^K y_{ik} \log p_{ik} + \frac{1}{|\mathcal{Q}|} \sum_{i \in \mathcal{Q}} \sum_{k=1}^K q_{ik} \log q_{ik} \\
&= \sum_{k=1}^K \hat{q}_k \log \hat{q}_k \\
&\quad + \frac{1 + \alpha}{2|\mathcal{Q}|} \sum_{i \in \mathcal{Q}} \sum_{k=1}^K q_{ik} \|\mathbf{z}_i - \mathbf{w}_k\|^2 + \frac{1 + \alpha}{|\mathcal{Q}|} \sum_{i \in \mathcal{Q}} \log \left(\sum_{j=1}^K e^{-\frac{1}{2} \|\mathbf{z}_i - \mathbf{w}_j\|^2} \right) \\
&\quad + \frac{\lambda}{2|\mathcal{S}|} \sum_{i \in \mathcal{S}} \sum_{k=1}^K y_{ik} \|\mathbf{z}_i - \mathbf{w}_k\|^2 + \frac{\lambda}{|\mathcal{S}|} \sum_{i \in \mathcal{S}} \log \left(\sum_{j=1}^K e^{-\frac{1}{2} \|\mathbf{z}_i - \mathbf{w}_j\|^2} \right) \\
&\quad + \frac{1}{|\mathcal{Q}|} \sum_{i \in \mathcal{Q}} \sum_{k=1}^K q_{ik} \log q_{ik} \quad (11)
\end{aligned}$$

Now, we can solve our problem approximately by alternating two sub-steps: one sub-step optimizes w.r.t classifier weights \mathbf{W} while auxiliary variables \mathbf{q} are fixed; another sub-step fixes \mathbf{W} and update \mathbf{q} .

- **W-update:** Omitting the terms that do not involve \mathbf{W} , Eq. (11) reads:

$$\underbrace{\frac{\lambda}{2|\mathcal{S}|} \sum_{i \in \mathcal{S}} y_{ik} \|\mathbf{z}_i - \mathbf{w}_k\|^2 + \frac{1+\alpha}{2|\mathcal{Q}|} \sum_{i \in \mathcal{Q}} q_{ik} \|\mathbf{z}_i - \mathbf{w}_k\|^2}_{\mathcal{C}:\text{convex}} + \underbrace{\frac{\lambda}{|\mathcal{S}|} \sum_{i \in \mathcal{S}} \log \left(\sum_{j=1}^K e^{-\frac{1}{2} \|\mathbf{z}_i - \mathbf{w}_j\|^2} \right) + \frac{1+\alpha}{|\mathcal{Q}|} \sum_{i \in \mathcal{Q}} \log \left(\sum_{j=1}^K e^{-\frac{1}{2} \|\mathbf{z}_i - \mathbf{w}_j\|^2} \right)}_{\bar{\mathcal{C}}:\text{non-convex}} \quad (12)$$

One can notice that objective (11) is not convex w.r.t \mathbf{w}_k . It can be split into convex and non-convex parts as in Eq. (12). Thus, we cannot simply set the gradients to 0 to get the optimal \mathbf{w}_k . The non-convex part can be linearized at the current $\mathbf{w}_k^{(t)}$ instead:

$$\bar{\mathcal{C}}(\mathbf{w}_k) \approx \bar{\mathcal{C}}(\mathbf{w}_k^{(t)}) + \frac{\partial \bar{\mathcal{C}}}{\partial \mathbf{w}_k}(\mathbf{w}_k^{(t)})^T (\mathbf{w}_k - \mathbf{w}_k^{(t)}) \quad (13)$$

$$\stackrel{\text{c}}{=} \frac{\lambda}{|\mathcal{S}|} \sum_{i \in \mathcal{S}} p_{ik}^{(t)} (\mathbf{z}_i - \mathbf{w}_k^{(t)})^T \mathbf{w}_k + \frac{1+\alpha}{|\mathcal{Q}|} \sum_{i \in \mathcal{Q}} p_{ik}^{(t)} (\mathbf{z}_i - \mathbf{w}_k^{(t)})^T \mathbf{w}_k \quad (14)$$

Where $\stackrel{\text{c}}{=}$ stands for "equal, up to an additive constant". By adding this linear term to the convex part \mathcal{C} , we can obtain a strictly convex objective in \mathbf{w}_k , whose gradients read w.r.t \mathbf{w}_k read

$$\frac{\partial(12)}{\partial \mathbf{w}_k} \approx \frac{\lambda}{|\mathcal{S}|} \left[\sum_{i \in \mathcal{S}} y_{ik} (\mathbf{z}_i - \mathbf{w}_k) + p_{ik}^{(t)} (\mathbf{z}_i - \mathbf{w}_k^{(t)}) \right] + \quad (15)$$

$$\frac{1+\alpha}{|\mathcal{Q}|} \left[\sum_{i \in \mathcal{Q}} q_{ik} (\mathbf{z}_i - \mathbf{w}_k) + p_{ik}^{(t)} (\mathbf{z}_i - \mathbf{w}_k^{(t)}) \right] \quad (16)$$

$$(17)$$

Setting those gradients to 0 recovers the optimal solution.

- **q-update:** With weights \mathbf{W} fixed, the objective is convex w.r.t auxiliary variables \mathbf{q}_i (sum of linear and convex functions) and the simplex constraints are affine. Therefore, one can minimize this constrained convex problem for each \mathbf{q}_i by solving the Karush-Kuhn-Tucker (KKT) conditions⁸. The KKT conditions yield closed-form solutions for both primal variable \mathbf{q}_i and the dual variable (Lagrange multiplier) corresponding to simplex constraint $\sum_{j=1}^K q_{ij} = 1$. Interestingly, the the negative entropy of auxiliary variables, i.e., $\sum_{k=1}^K q_{ik} \log q_{ik}$, which appears in the penalty term, handles implicitly non-negativity constraints $\mathbf{q}_i \geq 0$. In fact, this negative entropy acts as a barrier function, restricting the domain of each \mathbf{q}_i to non-negative values, which avoids extra dual variables and Lagrangian dual inner iterations for constraints $\mathbf{q}_i \geq 0$. As we will see, the closed-form solutions of the KKT conditions satisfy these non-negativity constraints, without explicitly imposing them. In addition to non-negativity, for each point i , we need to handle probability simplex constraints $\sum_{k=1}^K q_{ik} = 1$. Let $\gamma_i \in \mathbb{R}$ denote the Lagrangian multiplier corresponding to this constraint. The KKT conditions correspond to setting the following gradient of the Lagrangian function to zero, while enforcing the simplex constraints:

$$\frac{\partial \mathcal{L}}{\partial q_{ik}} = -\frac{1+\alpha}{|\mathcal{Q}|} \log p_{ik} + \frac{1}{|\mathcal{Q}|} (\log \hat{q}_k + 1) + \frac{1}{|\mathcal{Q}|} (\log q_{ik} + 1) + \gamma_i \quad (18)$$

$$= \frac{1}{|\mathcal{Q}|} \left(\log \left(\frac{q_{ik} \hat{q}_k}{p_{ik}^{1+\alpha}} \right) + 2 \right) + \gamma_i \quad (19)$$

This yields:

$$q_{ik} = \frac{p_{ik}^{1+\alpha}}{\hat{q}_k} e^{-(\gamma_i |\mathcal{Q}| + 2)} \quad (20)$$

⁸Note that strong duality holds since the objective is convex and the simplex constraints are affine. This means that the solutions of the (KKT) conditions minimize the objective.

Applying simplex constraint $\sum_{j=1}^K q_{ij} = 1$ to (20), Lagrange multiplier γ_i verifies:

$$e^{-(\gamma_i|\mathcal{Q}|+2)} = \frac{1}{\sum_{j=1}^K \frac{p_{ij}^{1+\alpha}}{\widehat{q}_j}} \quad (21)$$

Hence, plugging (21) in (20) yields:

$$q_{ik} = \frac{\frac{p_{ik}^{1+\alpha}}{\widehat{q}_k}}{\sum_{j=1}^K \frac{p_{ij}^{1+\alpha}}{\widehat{q}_j}} \quad (22)$$

Using the definition of \widehat{q}_k , we can decouple this equation:

$$\widehat{q}_k = \frac{1}{|\mathcal{Q}|} \sum_{i \in \mathcal{Q}} q_{ik} \propto \sum_{i \in \mathcal{Q}} \frac{p_{ik}^{1+\alpha}}{\widehat{q}_k} \quad (23)$$

which implies:

$$\widehat{q}_k \propto \left(\sum_{i=1}^N p_{ik}^{1+\alpha} \right)^{1/2} \quad (24)$$

Plugging this back in Eq. (22), we get:

$$q_{ik} \propto \frac{p_{ik}^{1+\alpha}}{\left(\sum_{i=1}^N p_{ik}^{1+\alpha} \right)^{1/2}} \quad (25)$$

Notice that $q_{ik} \geq 0$, hence the solution fulfils the positivity constraint of the original problem. □

C Details of ADM ablation

In Table 6, we provide the \mathbf{W} and \mathbf{q} updates for each configuration of the TIM-ADM ablation study, whose results were presented in Table 4. The proof for each of these updates is very similar to the proof of Proposition 2 detailed in Appendix B. Therefore, we do not detail it here.

Table 6: The \mathbf{W} and \mathbf{q} -updates for each case of the ablation study. "-" refers to the updates in Proposition 2. "NA" refers to non-applicable.

Loss	w_k update	q_{ik} update
CE	$\frac{\sum_{i \in \mathcal{S}} y_{ik} z_i}{\sum_{i \in \mathcal{S}} y_{ik}}$	N/A
CE + $\widehat{\mathcal{H}}(Y_{\mathcal{Q}} X_{\mathcal{Q}})$	-	$\propto p_{ik}^{1+\alpha}$
CE - $\widehat{\mathcal{H}}(Y_{\mathcal{Q}})$	-	$\propto \frac{p_{ik}}{\left(\sum_{i \in \mathcal{Q}} p_{ik} \right)^{1/2}}$
CE - $\widehat{\mathcal{H}}(Y_{\mathcal{Q}}) + \widehat{\mathcal{H}}(Y_{\mathcal{Q}} X_{\mathcal{Q}})$	-	-